The host galaxies of double compact objects across cosmic time

Mattia Toffano [1,2]★ Michela Mapelli [3,4,5,6] Nicola Giacobbo [3,4,5,6] M. Celeste Artale [5] and Giancarlo Ghirlanda [2]

[1]*Universitá degli Studi dell'Insubria, Via Valleggio 11, I-22100 Como, Italy*
[2]*INAF-Osservatorio Astronomico di Brera, Via E. Bianchi 46, I-23807 Merate, Italy*
[3]*INAF-Osservatorio Astronomico di Padova, Vicolo dell'Osservatorio 5, I-35122 Padova, Italy*
[4]*INFN, Milano Bicocca, Piazza della Scienza 3, I-20126 Milano, Italy*
[5]*Institut für Astro-und Teilchenphysik, Universität Innsbruck, Technikerstrasse 25/8, A-6020 Innsbruck, Austria*
[6]*Dipartimento di Fisica e Astronomia 'G. Galilei', Universitá di Padova, Vicolo dell'Osservatorio 3, I-35122 Padova, Italy*

ABSTRACT

We explore the host galaxies of compact-object binaries (black hole–black hole binaries, BHBs; neutron star–black hole binaries, NSBHs; double–neutron stars; DNSs) across cosmic time, by means of population-synthesis simulations combined with the Illustris cosmological simulation. At high redshift ($z \gtrsim 4$), the host galaxies of BHBs, NSBHs, and DNSs are very similar and are predominantly low-mass galaxies (stellar mass $M < 10^{11}$ M$_\odot$). If $z \gtrsim 4$, most compact objects form and merge in the same galaxy, with a short delay time. At low redshift ($z \leq 2$), the host galaxy populations of DNSs differ significantly from the host galaxies of both BHBs and NSBHs. DNSs merging at low redshift tend to form and merge in the same galaxy, with relatively short delay time. The stellar mass of DNS hosts peaks around $\sim 10^{10}$–10^{11} M$_\odot$. In contrast, BHBs and NSBHs merging at low redshift tend to form in rather small galaxies at high redshift and then to merge in larger galaxies with long delay times. This difference between DNSs and black hole binaries is a consequence of their profoundly different metallicity dependence.

Key words: black hole physics – gravitational waves – methods: numerical – stars: black holes – stars: mass-loss – stars: neutron.

1 INTRODUCTION

In 2015 September, the two advanced LIGO interferometers (Harry 2010; Aasi et al. 2015) obtained the first direct detection of gravitational waves (GWs) from a merging black hole–black hole binary (BHB; Abbott et al. 2016b). This detection was followed by other two BHB events during the first observing run (Abbott et al. 2016a,c), while the second observing run brought seven additional BHB mergers (Abbott et al. 2017a,b,f, 2018a) and one double–neutron star (DNS) merger (GW170817, Abbott et al. 2017c). The advanced Virgo interferometer (Acernese et al. 2015) joined the two advanced LIGO detectors in 2017 August, for the last part of O2, allowing for measurements of GW polarization and leading to a dramatic improvement of sky localization (Abbott et al. 2017b,c, 2018a, 2019). The third observing run of the LIGO–Virgo collaboration (LVC) has just started (2019 April 1): by the end of O3, we expect several tens of BHBs and few additional DNSs to enrich the current population of GW events.

GW170817 is the only event for which an electromagnetic counterpart was detected, covering almost the whole electromagnetic spectrum, from gamma to radio wavelengths (Abbott et al. 2017d,e; Abdalla et al. 2017; Alexander et al. 2017; Chornock et al. 2017; Coulter et al. 2017; Cowperthwaite et al. 2017; Goldstein et al. 2017; Hallinan et al. 2017; Margutti et al. 2017; Nicholl et al. 2017; Pian et al. 2017; Savchenko et al. 2017; Smartt et al. 2017; Soares-Santos et al. 2017; Troja et al. 2017; Valenti et al. 2017; Mooley et al. 2018; Ghirlanda et al. 2019). The counterpart has allowed us to uniquely identify the host galaxy as NGC 4993 (Coulter et al. 2017), an early-type massive galaxy at ∼40 Mpc distance from us (Blanchard et al. 2017; Fong et al. 2017; Im et al. 2017; Levan et al. 2017).

Shedding light on the properties of the host galaxies of black hole (BH) and neutron star (NS) binaries is a crucial step towards our understanding of the GW Universe (see e.g. Dvorkin et al. 2016; Lamberts et al. 2016; Mapelli et al. 2017; O'Shaughnessy et al. 2017; Schneider et al. 2017; Cao, Lu & Zhao 2018; Elbert, Bullock & Kaplinghat 2018; Lamberts et al. 2018; Mapelli & Giacobbo 2018; Artale et al. 2019). A good grasp on the properties of the host galaxies would enable us to test and improve different models of compact-binary formation, which are still affected by a plethora of uncertainties (see e.g. Tutukov & Yungelson 1973; Flannery & van den Heuvel 1975; Bethe & Brown 1998; Portegies Zwart &

★ E-mail: mattia.toffano@inaf.it

Yungelson 1998; Portegies Zwart & McMillan 2000; Belczynski, Kalogera & Bulik 2002; Voss & Tauris 2003; Podsiadlowski et al. 2004; Tauris & van den Heuvel 2006; Belczynski et al. 2007; Bogomazov, Lipunov & Tutukov 2007; Dominik et al. 2012, 2013, 2015; Mennekens & Vanbeveren 2014; de Mink & Belczynski 2015; Spera, Mapelli & Bressan 2015; Tauris, Langer & Podsiadlowski 2015; de Mink & Mandel 2016; Marchant et al. 2016; Mapelli et al. 2017; Chruslinska et al. 2018; Kruckow et al. 2018; Shao & Li 2018; Spera et al. 2019; Eldridge, Stanway & Tang 2019 or also Mapelli 2018, for a recent review). Furthermore, theoretical insights on the most likely properties of the host galaxies provide us with astrophysically motivated criteria for host localization. These criteria can facilitate the low-latency search for host candidates, by identifying the most probable hosts among the galaxies inside the error box (Del Pozzo et al. 2018). In addition, they can be used to 'rank' host candidates for those GW events in which we do not observe any electromagnetic counterpart (Mapelli et al. 2018).

Recent studies (Belczynski et al. 2016; Eldridge & Stanway 2016; Lamberts et al. 2016; Mapelli et al. 2017; Schneider et al. 2017; Marassi et al. 2019) focused on reconstructing the environment of GW150914 (see Abbott et al. 2016d) by accounting for the evolution of star formation rate density and metallicity (Z) across cosmic time. They conclude that GW150914 formed from metal-poor progenitors (most likely $Z \lesssim 0.1\,Z_\odot$, but possibly up to $Z \sim 0.5\,Z_\odot$, see Eldridge & Stanway 2016) either at low ($z \sim 0.2$) or high redshift ($z \gtrsim 2$).

Not only GW150914, but also the other merging binaries that are detected by GW detectors must not necessarily have formed in recent epochs: they may have formed in the early Universe and have merged after a long delay time (O'Shaughnessy, Kalogera & Belczynski 2010; Dominik et al. 2013, 2015; Mapelli et al. 2019). Hence, it is extremely important to learn when and in which circumstances these binaries did form.

Focusing on the host galaxies of BHBs, Schneider et al. (2017) suggest that most progenitors of GW150914-like events formed in dwarf galaxies (with stellar mass $M \lesssim 5 \times 10^6\,M_\odot$) while their merger occurred while they were hosted in a more massive galaxy ($M > 10^{10}\,M_\odot$). In contrast, DNSs are expected to form more likely in massive galaxies ($\gtrsim 10^9\,M_\odot$) at low redshift ($z \lesssim 0.024$) and tend to merge in the same galaxy where they formed (O'Shaughnessy et al. 2010; Mapelli et al. 2018; Artale et al. 2019). The explanation of this trend is that DNSs are poorly sensitive to progenitor stars' metallicity, while BHBs form preferentially from metal-poor stars (Perna & Belczynski 2002; Dominik et al. 2013; Giacobbo & Mapelli 2018a; Mapelli & Giacobbo 2018).

This paper is a follow-up of Mapelli et al. (2018). Following the same numerical approach as Mapelli et al. (2018), we interfaced the Illustris-1 cosmological simulation (Vogelsberger et al. 2014a) with catalogues of merging BHBs, DNSs, and neutron star–black hole binaries (NSBHs) simulated with the MOBSE population-synthesis code (Giacobbo, Mapelli & Spera 2018). While Mapelli et al. (2018) focused only on compact objects merging in the local Universe ($z \leq 0.024$), here we extend their analysis to compact objects merging across cosmic time. In particular, we explore the characteristics of the host galaxies of compact binaries at redshifts $z \sim 0, 2, 4$, and 6. In addition, we explore how these properties change across the cosmic time and search for possible relevant correlations that could arise among them. This information will be crucial in the next years with the upgrade of the advanced LIGO/Virgo interferometers to design sensitivity and for the next-generation ground-based GW detectors (Einstein Telescope, Cosmic Explorer; Sathyaprakash et al. 2012; Dwyer et al. 2015).

2 METHODS

2.1 MOBSE

MOBSE (Giacobbo et al. 2018) is an updated and customized version of the population-synthesis code BSE (Hurley, Tout & Pols 2002), which includes recent models of mass-loss by stellar winds (Vink et al. 2001; Vink & de Koter 2005), pair-instability and pulsational pair-instability supernovae (SNe; Spera & Mapelli 2017; Woosley 2017), core-collapse SNe (Fryer et al. 2012), and electron-capture SNe (Giacobbo & Mapelli 2018b). Specifically, mass-loss is described by an exponential law $\dot{M} \propto Z^\beta$, where $\beta = 0.85$ for Eddington ratio $\Gamma \leq 2/3$, $\beta = 2.45 - 2.4\Gamma$ for $2/3 \leq \Gamma < 1$, and $\beta = 0.05$ for $\Gamma > 1$ (Chen et al. 2015). Γ is the electron-scattering Eddington ratio, defined as (Gräfener et al. 2011)

$$\log \Gamma = -4.813 + \log(1 + X_H) + \log(L_\star/L_\odot) \\ - \log(M_\star/M_\odot), \tag{1}$$

where X_H is the Hydrogen fraction and $L_\star$ and $M_\star$ are, respectively, the star luminosity and the star mass. The mass distribution of BHs predicted by MOBSE shows a strong dependence on metallicity: Giacobbo et al. (2018) obtained BHs with maximum mass of the order of 60 $M_\odot$ for $Z \leq 0.001\,Z_\odot$, while the BH maximum mass at solar metallicity ($Z_\odot = 0.02$) is 25 $M_\odot$. The statistics and in particular the cosmic merger rate of compact-object binaries simulated by MOBSE are in agreement (Mapelli et al. 2017) with the values inferred by the LVC (Abbott et al. 2016a, 2017c, 2018a,b). For a more detailed description of MOBSE, see Giacobbo et al. (2018) and Giacobbo & Mapelli (2018b).

In this paper, we use the catalogue of merging compact objects from the run CC15α5 of Giacobbo & Mapelli (2018b). This simulation, in which a high value ($\alpha = 5$) for the efficiency of common-envelope ejection and a low value for SN kicks ($\sigma = 15\,\mathrm{km\,s^{-1}}$) are assumed, is the one that best matches the cosmic merger rate density of DNSs inferred by the LVC (Mapelli & Giacobbo 2018). Moreover, it matches the expected merger rate of DNSs in the Milky Way, estimated by Pol, McLaughlin & Lorimer (2019). The run CC15α5 consists of 1.2×10^8 stellar binaries, divided in 12 subsets, corresponding to different metallicities ($Z = 0.01, 0.02, 0.04, 0.06, 0.08, 0.1, 0.2, 0.3, 0.4, 0.6, 0.8$, and $1.0\,Z_\odot$ – here we assume $Z_\odot = 0.02$). We expect that our main results are not dramatically affected by the choice of the run CC15α5, since the other runs presented in Giacobbo & Mapelli (2018b) show a very similar trend with metallicity.

2.2 The Illustris

We convolve the outputs of MOBSE with the Illustris-1 simulation (hereafter, Illustris), which is the highest resolution run of the Illustris hydrodynamical cosmological simulation project (Vogelsberger et al. 2014a,b; Nelson et al. 2015). The simulation box's length is 106.5 Mpc, for an overall comoving volume of $(106.5)^3\,\mathrm{Mpc}^3$, with an initial baryonic and dark matter mass resolution of 1.26×10^6 and $6.26 \times 10^6\,M_\odot$, respectively. The Illustris box's size provides good resolution for massive haloes, while dwarf galaxies are predominantly unresolved. For more detailed information on the Illustris, see Vogelsberger et al. (2014a).

The Illustris includes subgrid physical models (e.g. for cooling, star formation, SNe, supermassive BH formation, accretion and merger, AGN feedback) as described in Vogelsberger et al. (2013). It is worth mentioning that the Illustris (like most cosmological simulations) does not include subgrid models for interacting binary

Table 1. Best-fitting parameters for the mass–metallicity relation obtained by Maiolino et al. (2008) at different redshifts.

z	$\log M_0$	K_0
0.07	11.18	9.04
0.7	11.57	9.04
2.2	12.38	8.99
3.5	12.28	8.69

stars in its stellar population models. The importance of interacting binaries in cosmological simulations deserves more investigation, but Wilkins et al. (2016) and Ma et al. (2016) both point out that feedback from interacting binaries plays a significant role in the high-redshift Universe. Moreover, the subgrid physical models adopted in the Illustris produce a mass–metallicity relation (Genel et al. 2014; Vogelsberger et al. 2014a; Genel 2016), which is steeper than the relation obtained through observational data (Torrey et al. 2014) and which does not show the turnover at stellar masses $\gtrsim 10^{10}$ M$_\odot$. In this paper, we thus substitute the simulation's intrinsic mass–metallicity relation with the one expected by observational data. In particular, we use the formula by Maiolino et al. (2008) and Mannucci et al. (2009):

$$12 + \log(\mathrm{O/H}) = -0.0864 (\log M - \log M_0)^2 + K_0, \qquad (2)$$

where M is the total stellar mass of the host galaxy in solar mass units, M_0 and K_0 are the parameters determined at each redshift by best fittings with observed data points (Table 1).

In equation (2), for redshifts $z > 3.5$ or $z < 0.07$ we use the same coefficients as for $z = 3.5$ and 0.07, respectively; for redshifts between the ones listed in the table, we adopt a linear interpolation. We extract the metallicity of each Illustris particle from a Gaussian distribution with mean value given by equation (2) and standard deviation $\sigma = 0.3$ dex to account for metallicity dispersion within galaxies. By repeating the calculations for a larger ($\sigma = 0.5$) and a smaller ($\sigma = 0.2$) scatter, we verified that our results are unchanged (see also Mapelli et al. 2017, 2018). To convert metallicities from O/H to Z, we assume that the solar metallicity is $Z_\odot = 0.02$. Hence, the solar value of $12 + \log(\mathrm{O/H})$ is equal to 8.92.

2.3 The Monte Carlo algorithm

We combined the catalogue of simulated compact-object binaries by MOBSE with the Illustris cosmological simulation through a Monte Carlo algorithm as follows. First, we extract the initial mass M_{Ill}, metallicity Z_{Ill}, and formation redshift z_{Ill} of each stellar particle in the Illustris. Secondly, we catalogue the masses of compact objects simulated by MOBSE and their delay time t_{delay} (i.e. the time elapsed between the formation of their progenitor stars and the merger). Finally, we use the following algorithm:

$$N_{\mathrm{CO,i}} = N_{\mathrm{BSE,i}}(Z \sim Z_{\mathrm{Ill}}) \frac{M_{\mathrm{Ill}}(Z_{\mathrm{Ill}})}{M_{\mathrm{BSE}}(Z \sim Z_{\mathrm{Ill}})} f_{\mathrm{corr}} f_{\mathrm{bin}} \qquad (3)$$

to associate a number $N_{\mathrm{CO,i}}$ of simulated compact-object binaries to each Illustris stellar particle (where $i = $ BHB, NSBH or DNS indicates the type of compact object). In equation (3), $M_{\mathrm{BSE}}(Z \sim Z_{\mathrm{Ill}})$ is the total initial mass of the stellar population simulated with MOBSE, which has metallicity Z closer to the one of the Illustris particle[1]

---

[1]It is worth mentioning that we match MOBSE metallicities and Illustris metallicities based on Z, i.e. the mass fraction of elements heavier than
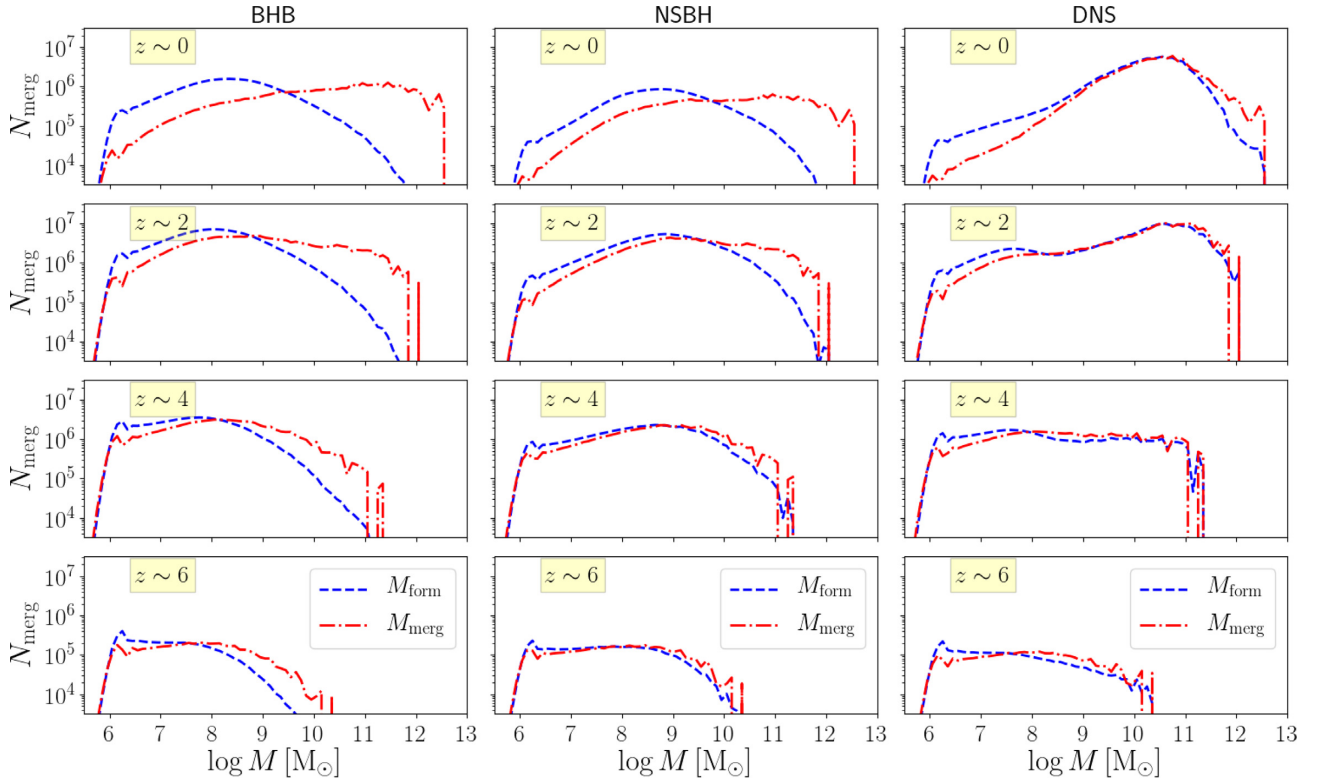
Z_{Ill} (with Z chosen among the 12 metallicities simulated with MOBSE), $N_{\mathrm{BSE,i}}(Z \sim Z_{\mathrm{Ill}})$ is the number of merging compact objects associated with the population of mass $M_{\mathrm{BSE}}(Z \sim Z_{\mathrm{Ill}})$, $f_{\mathrm{bin}} = 0.5$ is the assumed binary fraction, and $f_{\mathrm{corr}} = 0.285$ is a correction factor (to take into account that run CC15α5 contains only primary stars with zero-age main-sequence mass $M_{\mathrm{ZAMS}} > 5$ M$_\odot$).

We estimate for each compact-object binary the look-back time at which it merges as $t_{\mathrm{merg}} = t_{\mathrm{form}} - t_{\mathrm{delay}}$, where t_{form} is the look-back time at which the host Illustris particle formed:

$$t_{\mathrm{form}} = \frac{1}{H_0} \int_0^{z_{\mathrm{Ill}}} \frac{1}{(1+z)[\Omega_{\mathrm{M}}(1+z)^3 + \Omega_\Lambda]^{1/2}} \, \mathrm{d}z, \qquad (4)$$

where the cosmological parameters $H_0 = 100h$ km s^{-1} ($h = 0.704$), $\Omega_\Lambda = 0.7274$, and $\Omega_{\mathrm{M}} = 0.2726$ are the ones adopted in the Illustris (Hinshaw et al. 2013).

3 RESULTS

Through the formalism described in the previous section, we can analyse the main properties of the environment of merging compact objects, which are the stellar mass of host galaxy where the binary has formed (M_{form}), the stellar mass of the host galaxy where the merger occurs (M_{merg}), the delay times (t_{delay}), and the metallicity Z of the progenitor stars. We consider compact objects that reach coalescence in the Illustris snapshots corresponding to the redshift intervals $0.01 < z < 0.02$ (hereafter, $z \sim 0$), $2.00 < z < 2.10$ (hereafter, $z \sim 2$), $4.01 < z < 4.43$ (hereafter, $z \sim 4$), and $6.01 < z < 6.14$ (hereafter, $z \sim 6$) and formed previously.

Fig. 1 shows the distribution of M_{form} and M_{merg} for those BHBs, NSBHs, and DNSs that have formed at $z > 0.01$, $z > 2$, $z > 4$, and $z > 6$ and have merged in the Illustris snapshot corresponding to $z \sim 0$, 2, 4, and 6. At low redshifts, the mass M_{form} of the formation host of BHBs and NSBHs is typically lower than the mass M_{merg} of the galaxy where the merger occurred. This is not true for DNSs: both M_{form} and M_{merg} distributions peak around the same range (about 10^9–10^{11} M$_\odot$) even in the $z \sim 0$ case. These trends were already discussed in Mapelli et al. (2018): most BHBs and NSBHs merging at low z arise from metal-poor progenitors at high z. Thus, BHBs and NSBHs tend to form in smaller galaxies and to merge in larger ones, because of the hierarchical assembly of galaxies. In contrast, DNSs merging in the local Universe form predominantly from metal-rich progenitors with short delay time. Thus, they tend to form and merge in the same galaxy.

At $z \sim 2$, the difference between the distribution of M_{form} and M_{merg} becomes less marked and the maximum host mass is lower. This happens for two reasons: first, the time elapsed from the big bang to $z = 2$ is ~ 3 Gyr, so the largest galaxies did not have enough time to form (according to the hierarchical clustering model of galaxy assembly); secondly, following the same line of thought, even the delay time from the formation of a binary to its merger must be shorter than the $z \sim 0$ case and thus the mass of the formation host is closer to the mass of the merger host.

At $z \sim 4$, this trend is even stronger. In particular, almost all DNSs and most NSBHs form and merge in the same host galaxy.

Helium, but we estimated Illustris' metallicities based on [O/H] alone. This introduces another source of uncertainty in the models, because iron is the element that primarily affects stellar winds (Vink et al. 2001) and a measurement of [O/H] cannot be translated directly into [Fe/H], due to the fluctuations of the oxygen abundance with respect to the iron abundance (see e.g. the discussion in Eldridge et al. 2017).

Figure 1. Distribution of the stellar mass of the host galaxies where the compact binaries merge ($M_{\rm merg}$, red dot–dashed lines) and of the stellar mass of the host galaxies where their stellar progenitors formed ($M_{\rm form}$, blue dashed line). Left-hand column: BHBs; middle column: NSBHs; right-hand column: DNSs. From top to bottom: compact binaries merging at redshift $z \leq 0.01$, $z = 2.0$, $z = 4.0$, and $z = 6.0$, respectively.

The difference between the distribution of $M_{\rm form}$ and that of $M_{\rm merg}$ is significantly smaller even in the case of BHBs. Moreover, the distribution of DNS host masses, which peaked around $M_{\rm form} \sim M_{\rm merg} \sim 10^{11}$ M$_\odot$ at $z \sim 0$–2, is now rather flat.

The number of compact objects merging at $z \sim 6$ is significantly lower than at lower redshifts. While the $M_{\rm form}$ and $M_{\rm merg}$ distributions for NSBHs and DNSs are now almost identical, for BHBs we still see a small difference between $M_{\rm form}$ and $M_{\rm merg}$.

Galaxies with stellar mass $\lesssim 10^6$ M$_\odot$ are associated with just one Illustris stellar particle: smaller galaxies cannot form in the Illustris (see Schneider et al. 2017, for a different numerical approach that enables to study smaller dwarf galaxies). The spike we see in the $z \sim 2$ ($z \sim 4$) case around $\log M/{\rm M}_\odot = 12$ ($\log M/{\rm M}_\odot = 11.5$) is explained as a single massive galaxy being formed in the Illustris simulation. Finally, we notice that at $z \sim 2$ we have a higher total number of mergers compared to the other cases, due to the peak of star formation in this redshift range (Madau & Dickinson 2014). This trend is in agreement with previous papers (Dominik et al. 2013, 2015; Mapelli et al. 2017; Mapelli & Giacobbo 2018; Eldridge et al. 2019).

We now look for possible correlations between host galaxy mass, delay time, and metallicity of the compact binary. The left-hand panels of Fig. 2 show the metallicity Z of the progenitor as a function of the mass ratio $M_{\rm ratio} = M_{\rm merg}/M_{\rm form}$, while the right-hand panels show the delay time $t_{\rm delay}$ between the formation of the binary and the merger as a function of the mass ratio $M_{\rm ratio}$, for BHBs, NSBHs, and DNSs merging at $z = 0$.

It is apparent that DNSs lie in a different region of the $M_{\rm ratio} - Z$ plot with respect to BHBs and NSBHs. At $z \sim 0$, the vast majority of DNSs are characterized by a host mass ratio ~ 1, suggesting that

they formed and merged in the same galaxy, and by a progenitor metallicity in the range ~ 0.1–10 Z$_\odot$. In contrast, the host mass ratio for BHBs spans mainly over a large interval $M_{\rm ratio} \sim 1$–10^4 (i.e. $M_{\rm merg} \geq M_{\rm form}$), and the metallicity of their progenitors is always subsolar, with a preference for $Z \sim 0.02$–0.2 Z$_\odot$. NSBHs occupy approximately the same region as BHBs. As the latter, they never show a supersolar metallicity; on the other hand, a stronger preference for a smaller range of $M_{\rm ratio}$ (mainly ~ 1–10^3) is visible compared to BHBs. The number of merging NSBHs characterized by a $Z \leq 0.01$ Z$_\odot$ is very low (less than $<2 \times 10^3$).

We interpret this difference in terms of delay times (right-hand panels of Fig. 2): most BHBs merging at $z \sim 0$ form in smaller galaxies at high redshift and then merge at low redshift with a long delay time. Given the long BHB $t_{\rm delay}$, the initial host galaxy had enough time to grow in mass because of galaxy mergers and accretion. In contrast, most DNSs merging at $z \sim 0$ form in nearby galaxies and merge in the same galaxy with a short delay time. At $z \sim 0$, NSBHs mainly form in small galaxies at high redshift and merge after a long delay time, but we find also a good number of them forming in closer galaxies and merging within a shorter delay time. This interpretation is supported by the right-hand panel of Fig. 2, showing $t_{\rm delay}$ as a function of $M_{\rm ratio}$. The majority (~ 80 per cent) of DNSs merge within a $t_{\rm delay} < 4$ Gyr, while 65 per cent of BHBs have $t_{\rm delay} > 10$ Gyr. Around 20 per cent of NSBHs form and reach coalescence within $t_{\rm delay} \leq 4$ Gyr, while the ~ 40 per cent of them have $t_{\rm delay} > 10$ Gyr.

Fig. 3 is the same as Fig. 2 but for compact-object binaries merging at $z \sim 2$ (look-back time: 10.39 Gyr). In the upper panels, we notice that BHBs that merge at $z \sim 2$ are mainly characterized by an $M_{\rm ratio}$ of the order of tens. More specifically, ~ 50 per cent
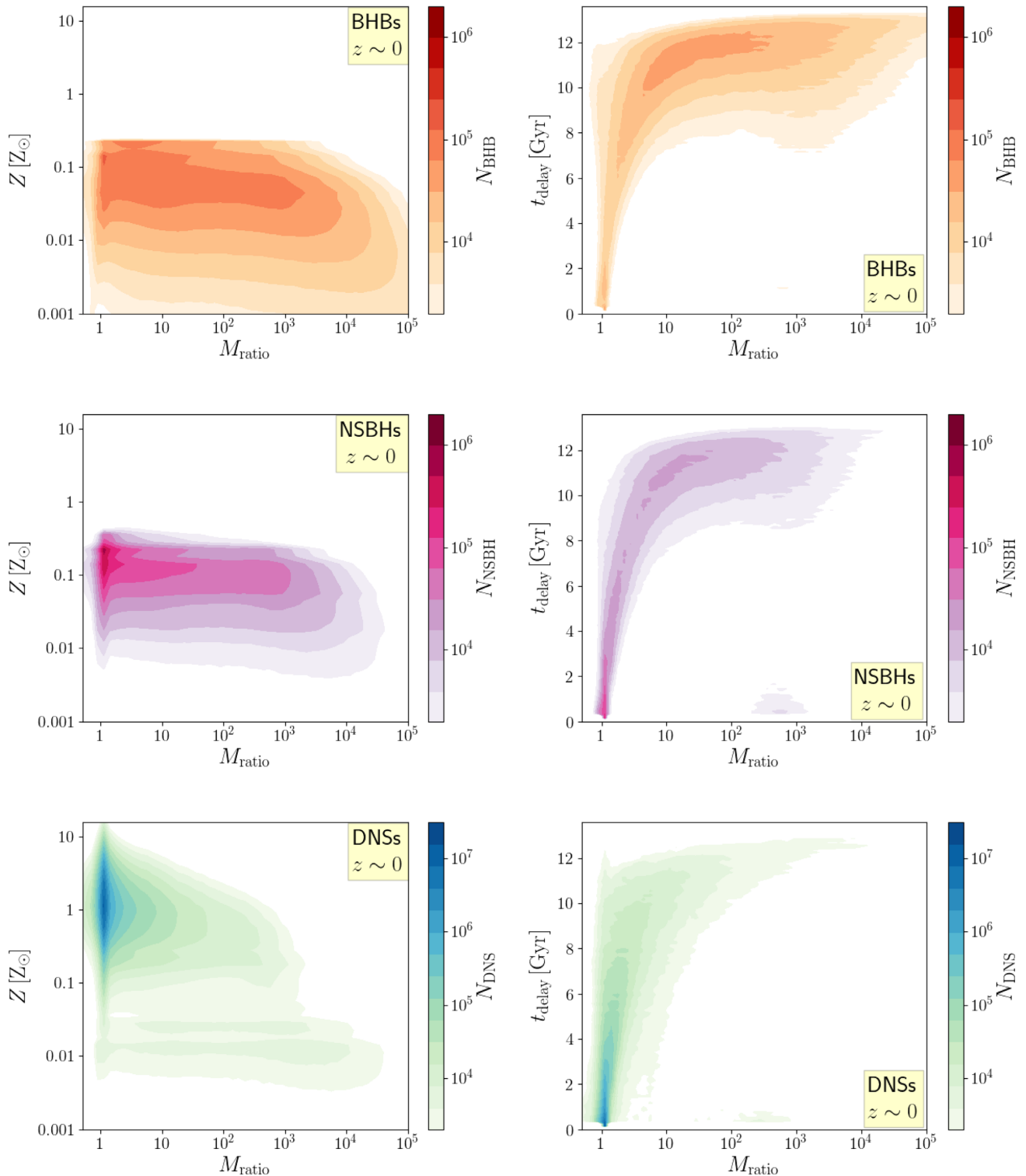
Figure 2. Left-hand panel: progenitor's metallicity versus ratio $M_{\mathrm{ratio}} = M_{\mathrm{merg}}/M_{\mathrm{form}}$ for DNSs (blue), NSBH (purple), and BHBs (orange) merging at $z \leq$ 0.01; right-hand panel: delay time t_{delay} versus M_{ratio} for DNSs (blue), NSBH (purple), and BHBs (orange) merging at $z \leq 0.01$. The colour-coded map (in logarithmic scale) indicates the number of merging compact objects per cell. Cells with $<2 \times 10^3$ compact-object binaries are shown in white. The cell sizes are $\log \delta Z/Z_\odot \times \log \delta M_{\mathrm{ratio}}/M_\odot = 0.1 \times 0.1$ and $\log \delta Z/Z_\odot \times \log \delta t_{\mathrm{delay}}/t_{\mathrm{delay}} = 0.1 \times 0.1$ for $M_{\mathrm{ratio}} - Z$ and $t_{\mathrm{delay}} - Z$ plots, respectively. Contour levels are spaced by a factor of $10^{0.3}$ binaries from each other.

of them merge within a mass ratio interval of 1–24, as reported in Table 2. The metallicity of BHB progenitors is always subsolar and in particular we have more progenitors with $Z < 0.01$ $Z_\odot$ with respect to the $z \sim 0$ case.

DNSs merging at $z \sim 2$ still show a preference for M_{ratio} ~ 1, but a significant number of objects have $M_{\mathrm{ratio}} \gg 1$. In particular, DNSs that form from metal-poor progenitors tend to have larger values of M_{ratio}. While most DNSs merging at $z \sim$
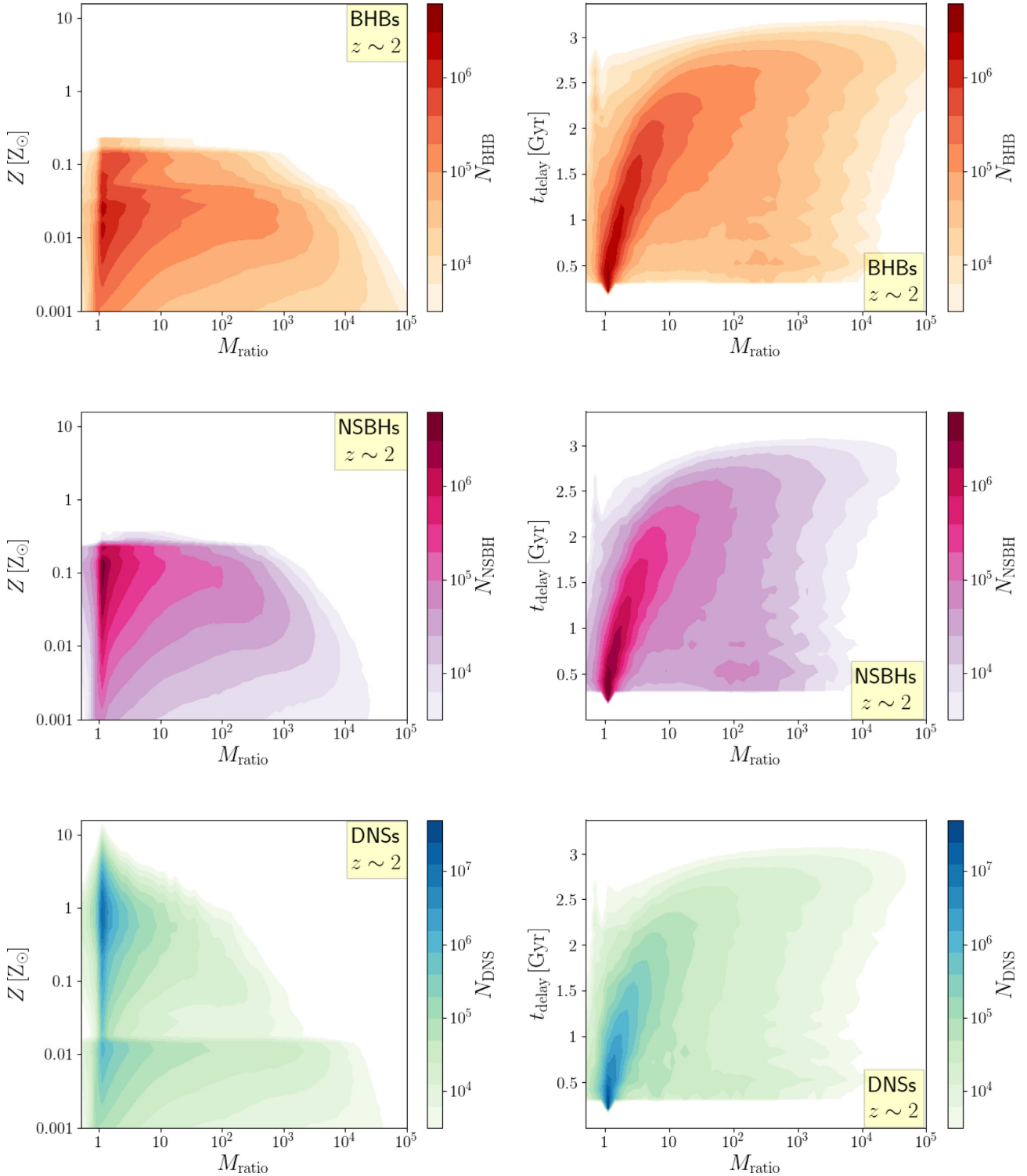
Figure 3. Same as Fig. 2, but for DNSs (bottom), NSBHs (middle), and BHBs (top) merging at redshift $z \sim 2$. Cells with $<3 \times 10^3$ compact-object binaries are shown in white.

2 have solar metallicity progenitors, the fraction of metal-poor progenitors increases significantly with respect to DNSs merging at $z \sim 0$. Metal-poor progenitors are also associated with slightly longer delay times.

From Table 2, we see that about half of NSBHs merging at $z \sim 2$ are characterized by an M_{ratio} of the order of one and are

thus associated with a short delay time. The remaining half are spread in an M_{ratio} interval spanning from ~ 10 to $\sim 10^4$. Likewise for DNSs, the number of metal-poor progenitors sensibly increased with respect to the $z \sim 0$ case.
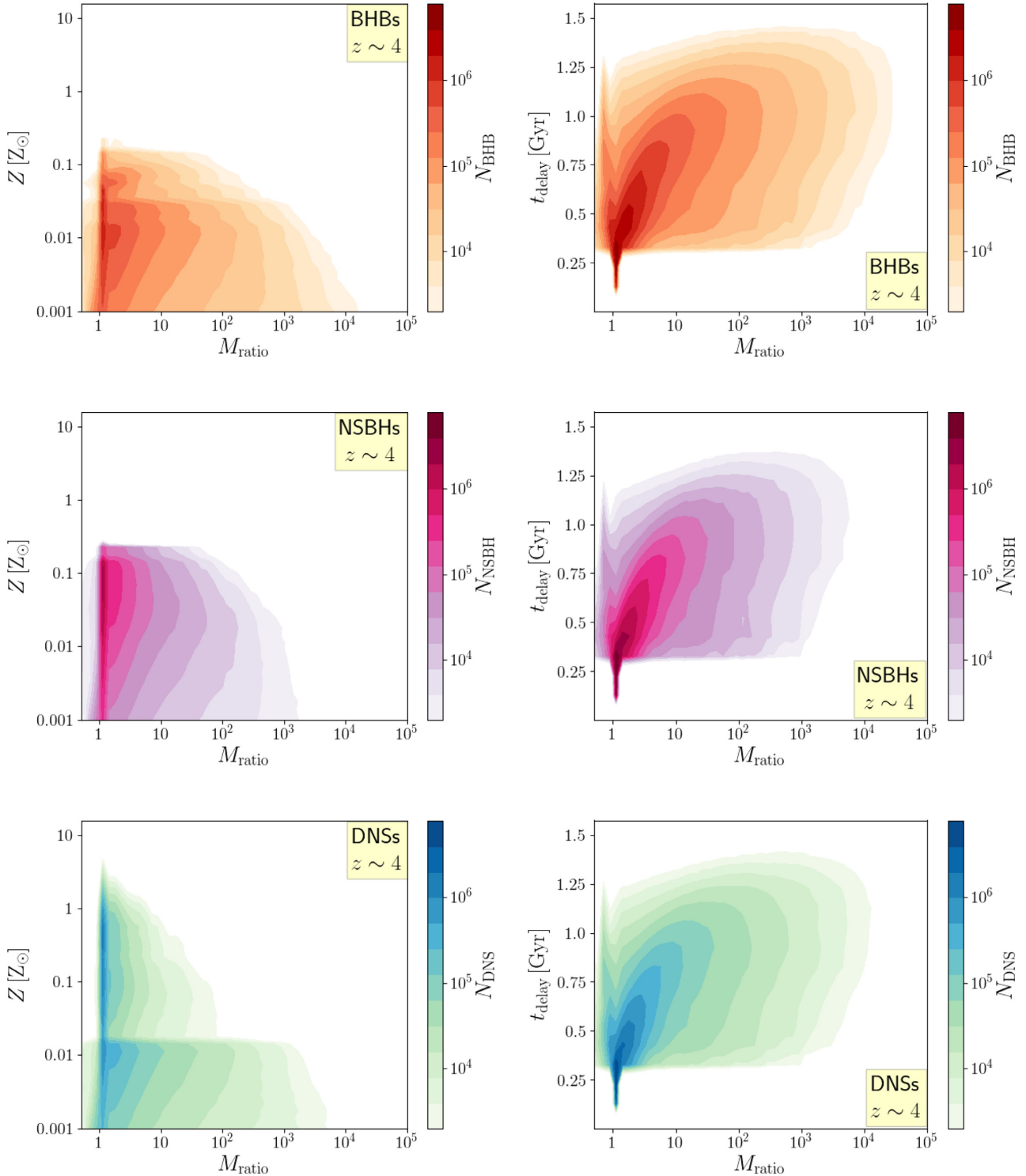
Fig. 4 is the same as Fig. 2 but for compact-object binaries merging at $z \sim 4$ (look-back time: 12.17 Gyr). BHB progenitors

Table 2. Mass ratio interval (in $M_\odot$) within which the 50 per cent of compact-object binaries merge at the distinct investigated redshifts.

	$z \sim 0$	$z \sim 2$	$z \sim 4$	$z \sim 6$
$M_{ratio, BHB}$	6.1–7.2×10^2	1.3–24	1–6.1	1–5
$M_{ratio, NSBH}$	1.5–1.6×10^2	1–5.8	1–2.4	0.9–1.9
$M_{ratio, DNS}$	1–2.7	0.9–1.5	1–2.7	1–3.5

squeeze to even lower metallicity. In particular, the vast majority of systems have $0.001 \leq Z/Z_\odot \leq 0.1$. Host mass ratios are sensibly smaller ($M_{ratio} \lesssim 6$ in the 50 per cent of cases), as it is reasonable to expect because the Universe is $\lesssim 1.5$ Gyr old.

The progenitors of DNSs merging at $z \sim 4$ shift to lower metallicities with respect to those merging at $z \sim 2$. The DNSs with metal-poor progenitors tend to have larger values of M_{ratio} and longer delay times than the DNSs with metal-rich progenitors.

Figure 4. Same as Fig. 2, but for DNSs (bottom), NSBHs (middle), and BHBs (top) merging at redshift $z \sim 4$.
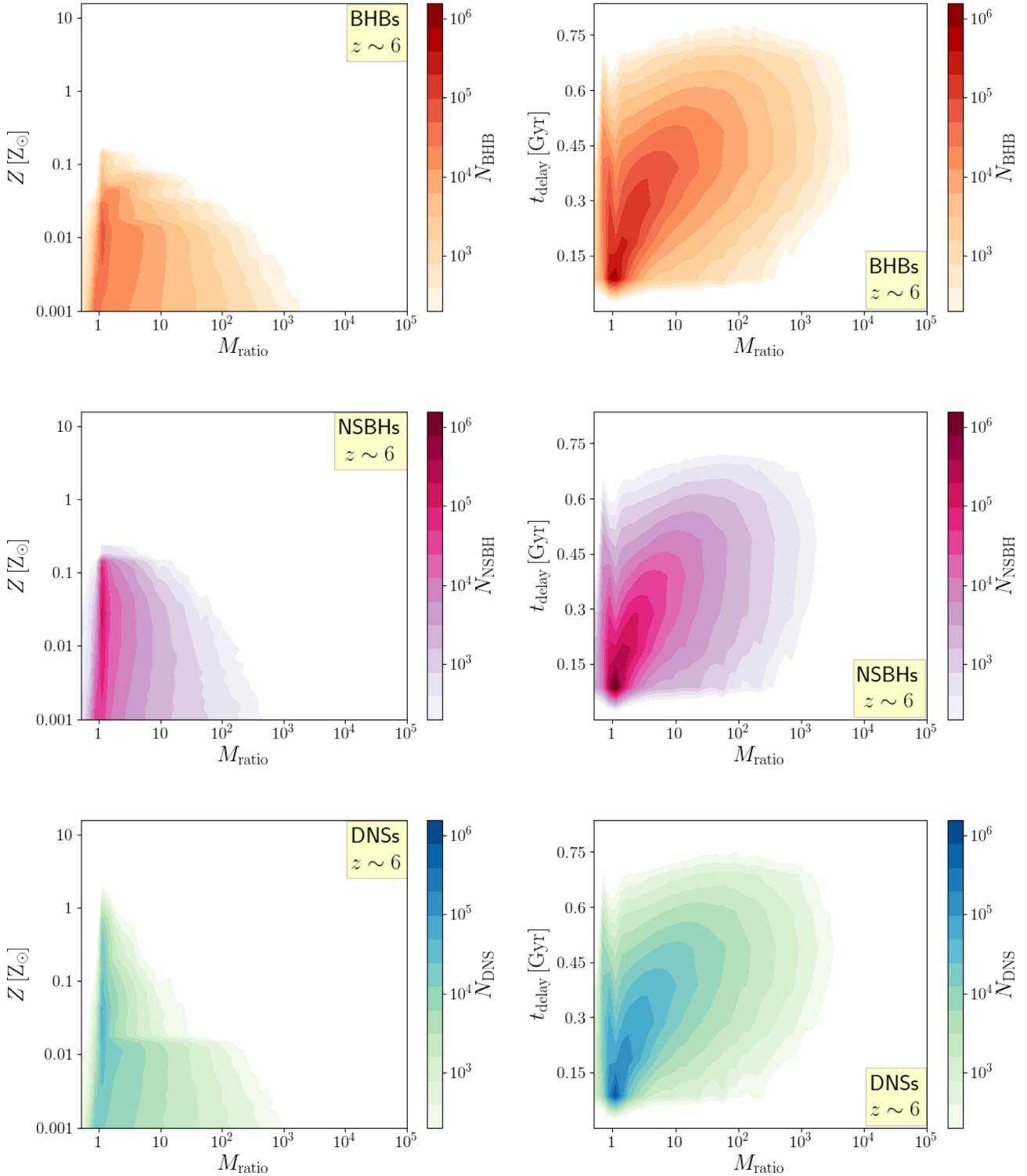
Figure 5. Same as Fig. 2 but for DNSs (bottom), NSBH (middle), and BHBs (top) merging at $z \sim 6$. Cells with $< 3 \times 10^2$ compact-object binaries are shown in white.

Hence, DNSs with metal-poor progenitors seem to behave more like BHBs than like the other DNSs.

Table 2 shows that 50 per cent of NSBHs merging at $z \sim 4$ have a narrow host mass ratio range, around ~ 1–2.4, which is related to a very short delay time.

Finally, Fig. 5 shows BHBs, NSBHs, and DNSs merging at $z \sim 6$ (look-back time: 12.797 Gyr). At such a high redshift, the number of mergers is much smaller than in the previous cases, because the cosmic star formation rate decreases quite fast for $z \geq 4$. The most noticeable feature in this figure is that all compact-object binaries

merging at $z \sim 6$ are very similar populations in terms of M_{ratio} and t_{delay}.

To summarize, our main result is that BHBs merging at low redshift are a significantly different population from DNSs merging at low redshift: the former have larger values of M_{ratio}, much smaller progenitor's metallicity, and much longer t_{delay} than the latter. As redshift increases, this difference becomes smaller: a subpopulation of DNSs with metal-poor progenitors and longer delay times appears at $z \sim 2$–4, well distinguished from the bulk of DNSs with metal-rich progenitors and short delay times. At high redshift $z \sim 6$, the population of merging DNSs is quite similar to the population of merging BHBs: both of them have mostly metal-poor progenitors and short delay times. The population of NSBHs shows a similar trend to BHBs at low redshift, in terms of M_{ratio}, t_{delay}, and progenitor's metallicity. With increasing redshift, M_{ratio} and t_{delay} shrink to values similar to DNSs, rather than BHBs. At $z \geq 2$, the main difference between NSBHs and DNSs is the metallicity range of progenitors.

4 DISCUSSION AND CONCLUSIONS

In this work, we have characterized the environment of merging compact objects across cosmic time, by means of population-synthesis simulations (run with the code MOBSE, Giacobbo & Mapelli 2018a; Giacobbo et al. 2018), combined with the Illustris cosmological simulation (Vogelsberger et al. 2014a,b; Nelson et al. 2015) through a Monte Carlo algorithm (Mapelli et al. 2017; Mapelli 2018).

We focused on the stellar mass of the host galaxy where the compact binaries merge, the stellar mass of the host galaxy where the progenitor stars formed, the metallicity of progenitor stars, and the delay time between the formation and the merger. We studied three types of compact-object binaries, BHBs, NSBHs, and neutron star–neutron star binaries (DNSs), for four reference epochs, corresponding to redshifts 0, 2, 4, and 6.

Present-day merging BHBs mainly formed $\sim$10–12 Gyr ago and merge in a more massive host galaxy than the one where they formed, due to the hierarchical clustering build-up process. In general, BHBs need a longer delay time to reach the merger phase compared to other compact-object binaries, even at higher redshifts. BHBs that merge nowadays have likely formed in galaxies with a mass $\sim 10^7$–10^{10} $M_\odot$ from metal-poor progenitors, but they merge in galaxies of every mass in the range 10^8–10^{12} $M_\odot$.

The difference between the mass of the formation host and the mass of the merger host becomes smaller and smaller as redshift increases (see Fig. 1). Lower masses of the formation hosts and lower metallicities of BHB progenitors are more likely going back in time, because smaller galaxies and metal-poor stars were more common in the past. This is a general trend, visible also for NSBHs and DNSs.

DNSs have a different behaviour with respect to BHBs. DNSs have a strong predisposition for high progenitor metallicities at any epochs (up to many times the solar value), and are characterized by low values of M_{ratio}, associated with short delay times. A secondary population of DNSs starts to emerge at $z \gtrsim 2$. This subpopulation is characterized by higher values of M_{ratio} and t_{delay} and metal-poor progenitors, similar to BHBs.

The current DNS host mass range (10^9–10^{11} $M_\odot$) is consistent with the mass range of short gamma-ray burst hosts (Fong et al. 2013), strengthening the link between DNS mergers and short gamma-ray bursts.

We foresee to find merging NSBHs at the present day mainly in galaxies within a mass range of $\sim 10^{7.5}$–$10^{10.5}$ $M_\odot$. The population of NSBHs merging at $z \sim 0$ shows a preference for small M_{ratio}, thus a tendency for shorter delay times; none the less, we find that many NSBH mergers are characterized by delay times of the order of 10 Gyr. At higher redshifts, M_{ratio} and t_{delay} squeeze to lower values, similar to DNSs. NSBHs are characterized by a subsolar metallicity of progenitors at each investigated epoch.

The $M_{ratio} - Z$ plots of DNSs (Figs 2–5) clearly show that there are two distinct subpopulations of DNSs: one with metallicity about solar (or above solar) and M_{ratio} strongly peaked around one, the other with metallicity $Z < 0.02$ $Z_\odot$ and with a broader distribution of M_{ratio}.

These two subpopulations arise from the population-synthesis model CC15α5 we adopted. Fig. 14 of Giacobbo & Mapelli (2018a) shows that in model CC15α5 DNSs born from metal-poor ($Z \lesssim 0.0004$) and metal-rich progenitors ($Z \gtrsim 0.01$) have approximately the same merger efficiency (defined as the number of mergers that we expect from a coeval stellar population integrated over the Hubble time), while the merger efficiency drops by a factor of $\sim$5–10 for DNSs with intermediate-metallicity progenitors ($Z \approx 0.002$).

In conclusion, our study suggests that the mass of the host galaxies encodes important information on the populations of merging compact objects across cosmic time. Upcoming third-generation ground-based GW detectors will be able to observe DNS mergers up to $z \geq 2$ and BHB mergers up to $z \geq 10$, unveiling the properties of merging compact objects as a function of redshift (Kalogera et al. 2019). Our results can provide a criterion to rank possible host galaxies of GW events (within the LIGO–Virgo error box), based on their mass and redshift. When fed into a low-latency search pipeline (e.g. Del Pozzo et al. 2018), this information might improve the responsiveness of the search for electromagnetic counterparts. In absence of a counterpart, our results can be used as criteria to identify the most likely host galaxies within the LIGO–Virgo error box.

In preparation for the era of third-generation GW detectors, we show that characterizing the environment and the host mass of compact-object binaries at high redshift is crucial to identify the population of their progenitor stars.

REFERENCES

Aasi J. et al., 2015, Class. Quantum Gravity, 32, 115012
Abbott B. P. et al., 2016a, Phys. Rev. X, 6, 041015
Abbott B. P. et al., 2016b, Phys. Rev. Lett., 116, 061102
Abbott B. P. et al., 2016c, Phys. Rev. Lett., 116, 241103
Abbott B. P. et al., 2016d, ApJ, 818, L22
Abbott B. P. et al., 2017a, Phys. Rev. Lett., 118, 221101
Abbott B. P. et al., 2017b, Phys. Rev. Lett., 119, 141101
Abbott B. P. et al., 2017c, Phys. Rev. Lett., 119, 161101
Abbott B. P. et al., 2017d, ApJ, 848, L12

Abbott B. P. et al., 2017e, ApJ, 848, L13
Abbott B. P. et al., 2017f, ApJ, 851, L35
Abbott B. P. et al., 2018a, Phys. Rev. X, 9, 031040
Abbott B. P. et al., 2018b, preprint (arXiv:1811.12940)
Abbott B. P. et al., 2019, ApJ, 875, 161
Abdalla H. et al., 2017, ApJ, 850, L22
Acernese F. et al., 2015, Class. Quantum Gravity, 32, 24001
Alexander K. D. et al., 2017, ApJ, 848, L21
Artale M. C., Mapelli M., Giacobbo N., Sabha N. B., Spera M., Santoliquido
    F., Bressan A., 2019, MNRAS, 487, 1675
Belczynski K., Kalogera V., Bulik T., 2002, ApJ, 572, 407
Belczynski K., Taam R. E., Kalogera V., Rasio F. A., Bulik T., 2007, ApJ,
    662, 504
Belczynski K., Holz D. E., Bulik T., O'Shaughnessy R., 2016, Nature, 534,
    512
Bethe H. A., Brown G. E., 1998, ApJ, 506, 780
Blanchard P. K. et al., 2017, ApJ, 848, L22
Bogomazov A. I., Lipunov V. M., Tutukov A. V., 2007, Astron. Rep., 51,
    308
Cao L., Lu Y., Zhao Y., 2018, MNRAS, 474, 4997
Chen Y., Bressan A., Girardi L., Marigo P., Kong X., Lanza A., 2015,
    MNRAS, 452, 1068
Chornock R. et al., 2017, ApJ, 848, L19
Chruslinska M., Belczynski K., Klencki J., Benacquista M., 2018, MNRAS,
    474, 2937
Coulter D. A. et al., 2017, Science, 358, 1556
Cowperthwaite P. S. et al., 2017, ApJ, 848, L17
de Mink S. E., Belczynski K., 2015, ApJ, 814, L17
de Mink S. E., Mandel I., 2016, MNRAS, 460, 3545
Del Pozzo W., Berry C. P. L., Ghosh A., Haines T. S. F., Singer L. P., Vecchio
    A., 2018, MNRAS, 479, 601
Dominik M., Belczynski K., Fryer C., Holz D. E., Berti E., Bulik T., Mandel
    I., O'Shaughnessy R., 2012, ApJ, 759, 52
Dominik M., Belczynski K., Fryer C., Holz D. E., Berti E., Bulik T., Mandel
    I., O'Shaughnessy R., 2013, ApJ, 779, 72
Dominik M. et al., 2015, ApJ, 806, 263
Dvorkin I., Vangioni E., Silk J., Uzan J.-P., Olive K. A., 2016, MNRAS,
    461, 3877
Dwyer S., Sigg D., Ballmer S. W., Barsotti L., Mavalvala N., Evans M.,
    2015, Phys. Rev. D, 91, 082001
Elbert O. D., Bullock J. S., Kaplinghat M., 2018, MNRAS, 473, 1186
Eldridge J. J., Stanway E. R., 2016, MNRAS, 462, 3302
Eldridge J. J., Stanway E. R., Xiao L., McClelland L. A. S., Taylor G., Ng
    M., Greis S. M. L., Bray J. C., 2017, Publ. Astron. Soc. Aust., 34, e058
Eldridge J. J., Stanway E. R., Tang P. N., 2019, MNRAS, 482, 870
Flannery B. P., van den Heuvel E. P. J., 1975, A&A, 39, 61
Fong W. et al., 2013, ApJ, 769, 56
Fong W. et al., 2017, ApJ, 848, L23
Fryer C. L., Belczynski K., Wiktorowicz G., Dominik M., Kalogera V., Holz
    D. E., 2012, ApJ, 749, 91
Genel S. et al., 2014, MNRAS, 445, 175
Genel S., 2016, ApJ, 822, 107
Ghirlanda G. et al., 2019, Science, 363, 968
Giacobbo N., Mapelli M., 2018a, MNRAS, 480, 2011
Giacobbo N., Mapelli M., 2018b, MNRAS, 482, 2234
Giacobbo N., Mapelli M., Spera M., 2018, MNRAS, 474, 2959
Goldstein A. et al., 2017, ApJ, 848, L14
Gräfener G., Vink J. S., de Koter A., Langer N., 2011, A&A, 535, A56
Hallinan G. et al., 2017, Science, 358, 1579
Harry G. M., 2010, Class. Quantum Gravity, 27, 084006
Hinshaw G. et al., 2013, ApJS, 208, 2
Hurley J. R., Tout C. A., Pols O. R., 2002, MNRAS, 329, 897
Im M. et al., 2017, ApJ, 849, L16
Kalogera V. et al., 2019, BAAS, 51, 242
Kruckow M. U., Tauris T. M., Langer N., Kramer M., Izzard R. G., 2018,
    MNRAS, 481, 1908
Lamberts A., Garrison-Kimmel S., Clausen D. R., Hopkins P. F., 2016,
    MNRAS, 463, L31

Lamberts A. et al., 2018, MNRAS, 480, 2704
Levan A. J. et al., 2017, ApJ, 848, L28
Ma X., Hopkins P. F., Kasen D., Quataert E., Faucher-Giguère C.-A., Kereš
    D., Murray N., Strom A., 2016, MNRAS, 459, 3614
Madau P., Dickinson M., 2014, ARA&A, 52, 415
Maiolino R. et al., 2008, A&A, 488, 463
Mannucci F. et al., 2009, MNRAS, 459, 3432
Mapelli M., 2018, preprint (arXiv:1809.09130)
Mapelli M., Giacobbo N., 2018, MNRAS, 479, 4391
Mapelli M., Giacobbo N., Ripamonti E., Spera M., 2017, MNRAS, 472,
    2422
Mapelli M., Giacobbo N., Toffano M., Ripamonti E., Bressan A., Spera M.,
    Branchesi M., 2018, MNRAS, 481, 5324
Mapelli M., Giacobbo N., Santoliquido F., Artale M. C., 2019, MNRAS,
    487, 2
Marassi S., Graziani L., Ginolfi M., Schneider R., Mapelli M., Spera M.,
    Alparone M., 2019, MNRAS, 484, 3219
Marchant P., Langer N., Podsiadlowski P., Tauris T. M., Moriya T. J., 2016,
    A&A, 588, A50
Margutti R. et al., 2017, ApJ, 848, L20
Mennekens N., Vanbeveren D., 2014, A&A, 564, A134
Mooley K. P. et al., 2018, ApJ, 868, L11
Nelson D. et al., 2015, Astron. Comput., 13, 12
Nicholl M. et al., 2017, ApJ, 848, L18
O'Shaughnessy R., Kalogera V., Belczynski K., 2010, ApJ, 716, 615
O'Shaughnessy R., Bellovary J. M., Brooks A., Shen S., Governato F.,
    Christensen C. R., 2017, MNRAS, 464, 2831
Perna R., Belczynski K., 2002, ApJ, 570, 252
Pian E. et al., 2017, Nature, 551, 67
Podsiadlowski P., Langer N., Poelarends A. J. T., Rappaport S., Heger A.,
    Pfahl E., 2004, ApJ, 612, 1044
Pol N., McLaughlin M., Lorimer D. R., 2019, ApJ, 870, 71
Portegies Zwart S. F., McMillan S. L. W., 2000, ApJ, 528, L17
Portegies Zwart S. F., Yungelson L. R., 1998, A&A, 332, 173
Sathyaprakash B. et al., 2012, Class. Quantum Gravity, 29, 124013
Savchenko V. et al., 2017, ApJ, 848, L15
Schneider R., Graziani L., Marassi S., Spera M., Mapelli M., Alparone M.,
    Bennassuti M. d., 2017, MNRAS, 471, L105
Shao Y., Li X.-D., 2018, MNRAS, 477, L128
Smartt S. J. et al., 2017, Nature, 551, 75
Soares-Santos M. et al., 2017, ApJ, 848, L16
Spera M., Mapelli M., 2017, MNRAS, 470, 4739
Spera M., Mapelli M., Bressan A., 2015, MNRAS, 470, 4739
Spera M., Mapelli M., Giacobbo N., Trani A. A., Bressan A., Costa G.,
    2019, MNRAS, 485, 889
Tauris T. M., van den Heuvel E. P. J., 2006, in Lewin W., Van der Klis M., eds,
    Formation and evolution of compact stellar X-ray sources. Cambridge
    Univ. Press, Cambridge, p. 623
Tauris T. M., Langer N., Podsiadlowski P., 2015, MNRAS, 451, 2123
Torrey P., Vogelsberger M., Genel S., Sijacki D., Springel V., Hernquist L.,
    2014, MNRAS, 438, 1985
Troja E. et al., 2017, Nature, 551, 71
Tutukov A., Yungelson L., 1973, Nauchnye Inf., 27, 70
Valenti S. et al., 2017, ApJ, 848, L24
Vink J. S., de Koter A., 2005, A&A, 442, 587
Vink J. S., de Koter A., Lamers H. J. G. L. M., 2001, A&A, 369, 574
Vogelsberger M., Genel S., Sijacki D., Torrey P., Springel V., Hernquist L.,
    2013, MNRAS, 436, 3031
Vogelsberger M. et al., 2014a, MNRAS, 444, 1518
Vogelsberger M. et al., 2014b, Nature, 509, 177
Voss R., Tauris T. M., 2003, MNRAS, 342, 1169
Wilkins S. M., Feng Y., Di-Matteo T., Croft R., Stanway E. R., Bouwens R.
    J., Thomas P., 2016, MNRAS, 458, L6
Woosley S. E., 2017, ApJ, 836, 244

This paper has been typeset from a T_EX/L^AT_EX file prepared by the author.